

***Investigation of prompt fission neutron (PFN)  
emission in  $^{235}\text{U}(n_{th}, f)$  reaction***

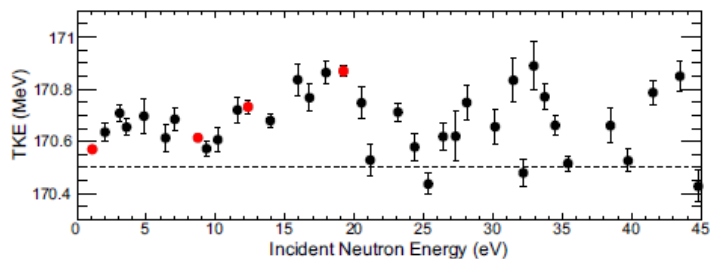
***Zeynalov Sh. Sedyshev P., Sidorova O., Shvetsov V.***

***JINR-Joint Institute for Nuclear Research, Dubna, Russia***

**The mechanism of PFN emission in fission plays important role in nuclear fission theory from the one hand and the information on PFN is highly demanded by nuclear power industry from the other hand.**

**Analysis of angular distribution of PFN measured in resonance neutron induced fission of  $^{235}\text{U}$  revealed surprisingly high anisotropy of PFN in FF centre-of-mass reference frame!? This results were confirmed by recent investigation of dr F.-J. Hamsch team.**

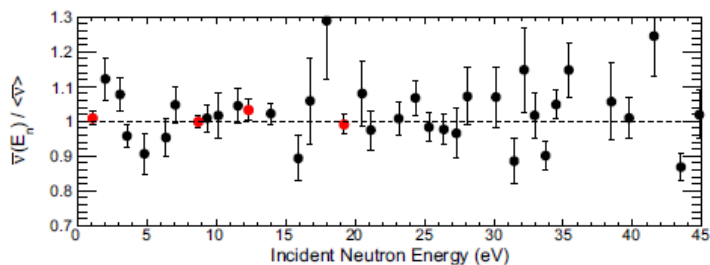
**In current report we presenting some preliminary results of test measurement of PFN emission in thermal neutron induced fission of  $^{235}\text{U}$  target as test of apparatus for resonance neutron induced fission of  $^{235}\text{U}$  at IREN facility**



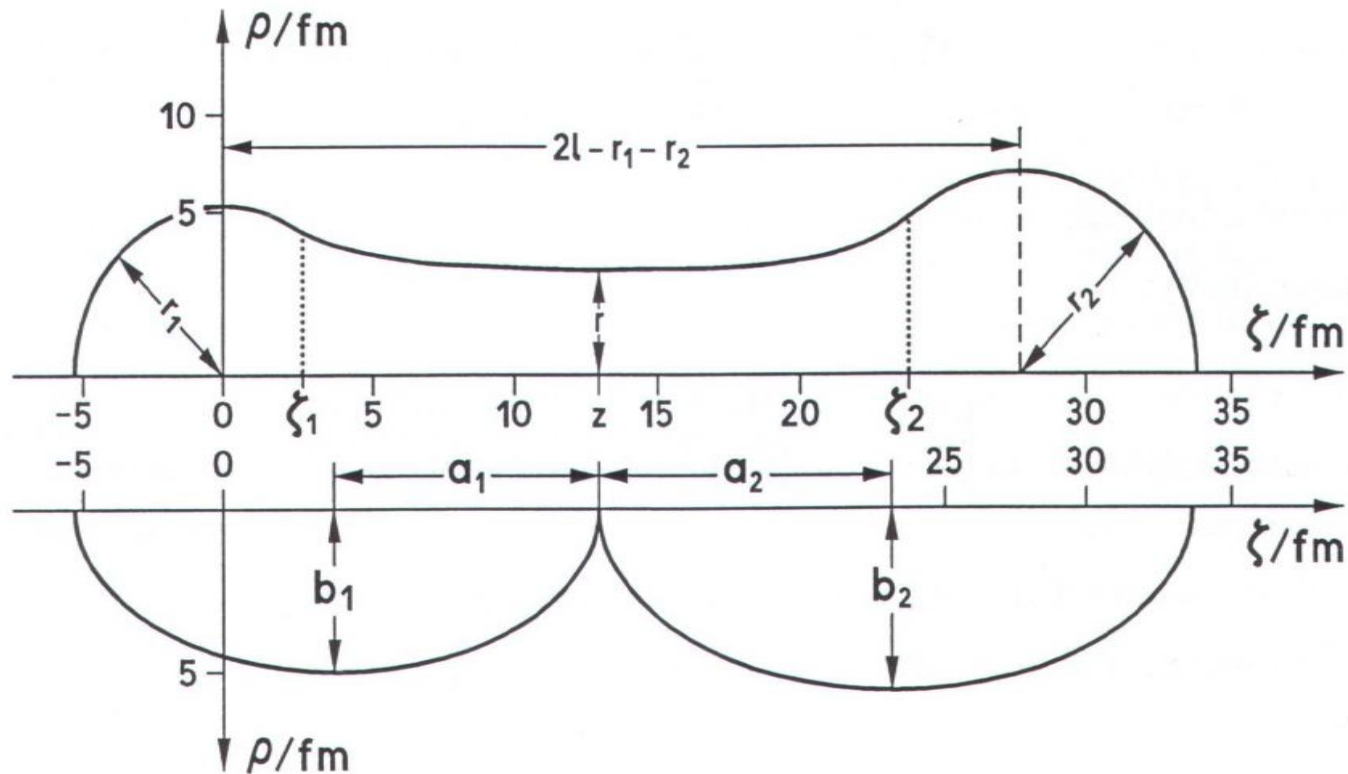
EPJ Web of Conferences **111**, 05001 (2016)

DOI: 10.1051/epjconf/201611105001

© Owned by the authors, published by EDP Sciences, 2016

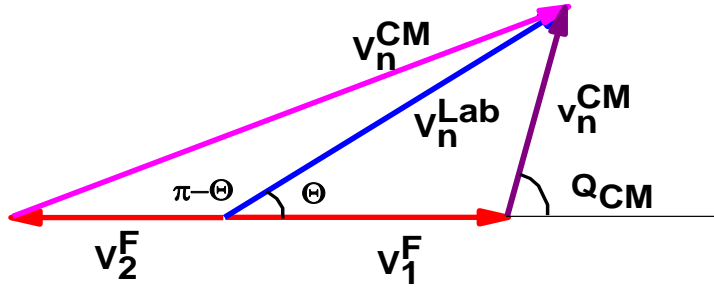


## Pre-scission nuclear shape parameterization in MM-RNR and PFN emission



PFN emission mechanism in MM-RNR is considered as RNR, leading to the excited FFs. PFN emission is the first stage of FFs de-excitation, following by  $\gamma$ -ray emission.

# PFN emission kinematics

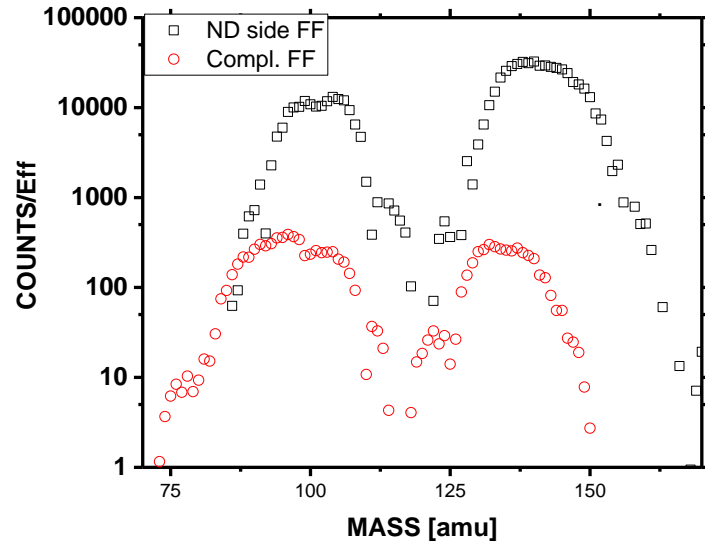


$$(V_n^{CM})^2 = (V_2^F)^2 + (V_n^{Lab})^2 + 2 \cdot V_2^F \cdot V_n^{Lab} \cdot \cos(\Theta)$$

$$(v_n^{CM})^2 = (V_1^F)^2 + (V_n^{Lab})^2 - 2 \cdot V_1^F \cdot V_n^{Lab} \cdot \cos(\Theta)$$

$$v_n^{CM} \cdot \cos(Q_{CM}) = V_n^{Lab} \cdot \cos(\Theta) - V_1^F$$

$$\Omega_{CM}(v_{CM}, \Theta_{CM}) dv_{CM} d \cos(\Theta_{CM}) = \frac{v_{CM}}{v_{lab}} \Omega_{lab}(v_{lab}, g(v_{CM}, \Theta_{CM}))$$

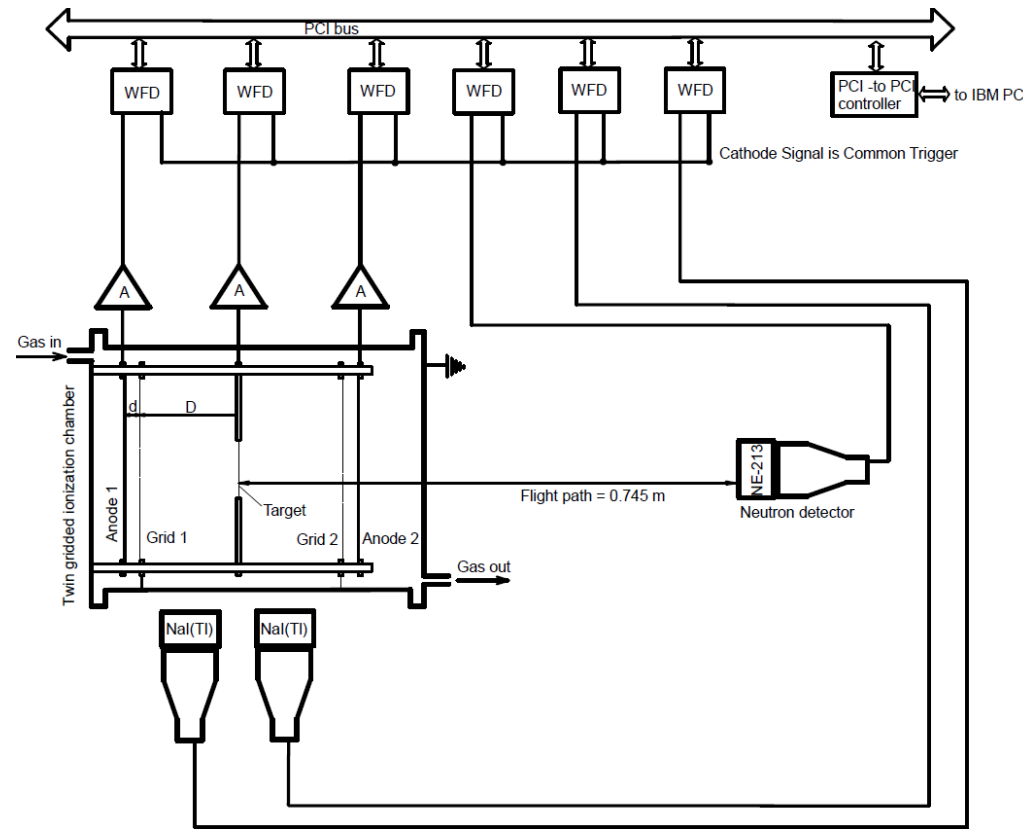


$$h_H = \left(\frac{1}{T}\right) \exp(-E_H^{CM} / T)$$

$$h_L = \left(\frac{1}{T}\right) \exp(-E_L^{CM} / T)$$

$$h_L + h_H = 1$$

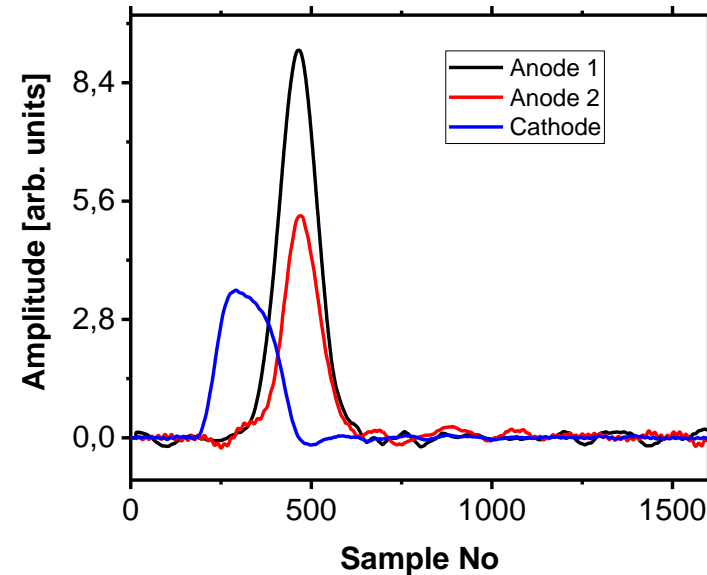
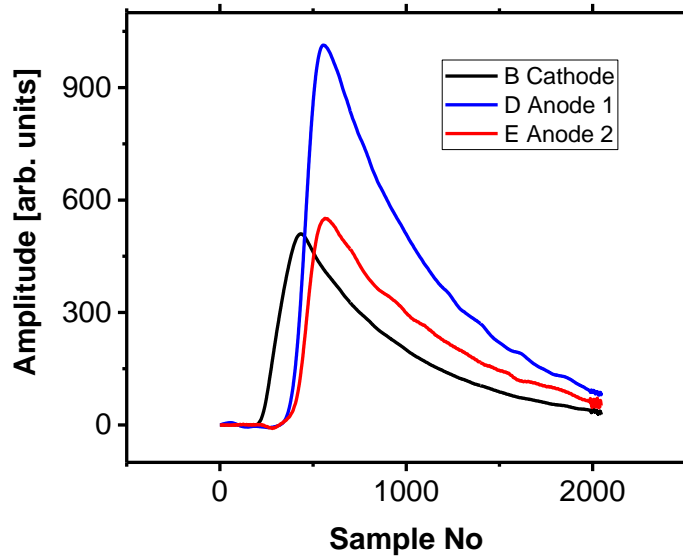
# 1. Experimental setup and acquisition system.



Goal of this work was mass and TKE dependence of PFN distribution measurement in reaction. We adopted the approach of C. Budtz-Jorgensen and K.-H. Knitter, where it can be done by measurement mass yield versus TKE in two measurements with and without demanding coincidence between FF and PFN emission. Thanks to developments in electronics, digital pulse processing, and PFN detection techniques we managed to modify B-K approach and in this presentation we report some modifications related to software and mathematics of digital pulse processing application fission. We also have developed some automation of data analysis process bearing in mind to accelerate very cumbersome data analysis procedure. Implementation of data analysis procedure was based on adaptation methods of analogue pulse processing, which we understood as linear mathematical operators to continuous signals.

Adopted from C. Budtz-Jørgensen and H.-H. Knitter, *Nucl. Phys.*, A490, 307(1988) and modified with digital pulse processing apparatus

### 3. Digital Pulse Processing (DPP).



According to Shannon sampling theorem both continuous and sampled representations are equivalent if the sampling of continuous signal made with appropriate frequency. Then the analysis, implemented to experimental data, should provide the correct results. In our approach we have oversampled FF signals. The oversampling we used to increase the effective number of bits (ENOB) improving the signal representation. In practice the increase of ENOB realized automatically when signal passed through second order low pass filter :

$$V_{out}^1(t) = \int_0^{\infty} V_{in}(\xi) \cdot \exp\left(-\frac{(\xi-t)}{\tau}\right) d\xi, \quad V_{out}^2 = \int_0^{\infty} V_{out}^1(\xi) \cdot \exp\left(-\frac{(\xi-t)}{\tau}\right) d\xi$$

Improved signal presentation (left figure) facilitates numerical solution of the integral equation

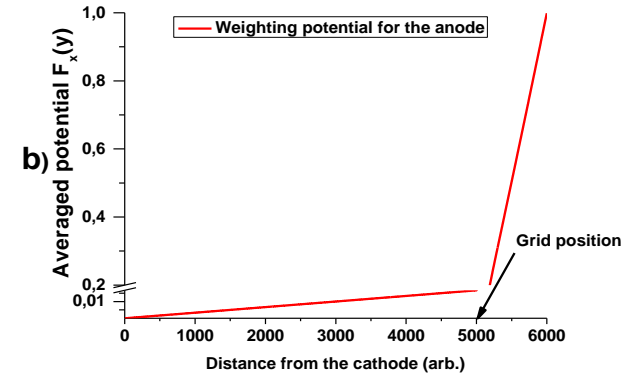
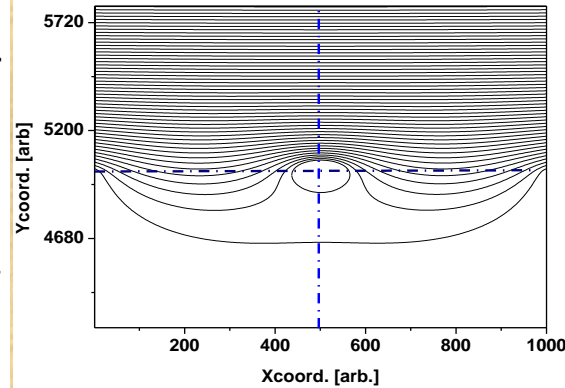
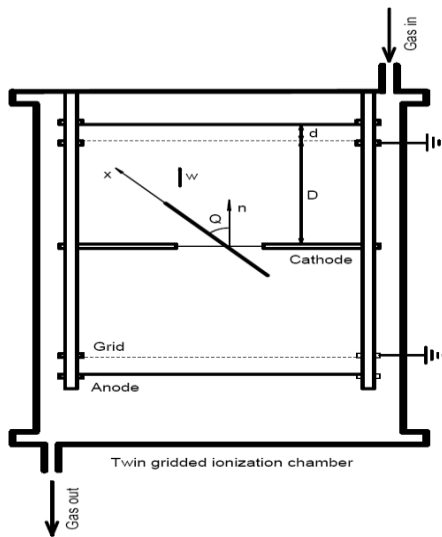
$$V(t) = Const \cdot \int_0^t i(\xi) \exp(-\xi/\tau) d\xi$$

Solution of above eq.  $i(t)$  presented on the right figure for the cathode and two anode signals. In terms of familiar analog electronics the operation performed equivalent to differential filter on the input of spectroscopy amplifier (SA). To simulate integrating stage of the SA we implemented integration according to

$$V(t) = \int_0^t i(\xi) d\xi$$

The last operation performed with two correlated anode waveforms provides the pulse heights of FF.

## 4. Drift time determination of FF ionization



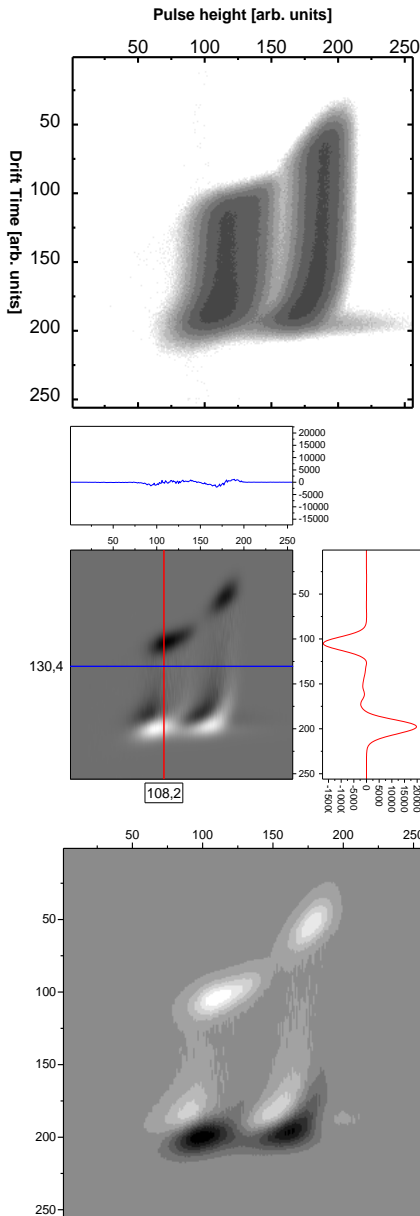
Theorem and the concepts of the weighting field and weighting potential states that the instantaneous current induced on a given electrode is equal to  $i = q\bar{v}E_0$ , where  $q$  is the charge of the carrier,  $\bar{v}$  is its velocity, and  $E_0$  is called the weighting field. Another way of stating the same principle is that the induced charge on the electrode is given by the product of the charge on the carrier multiplied by the difference in the weighting potential from the beginning to the end of the carrier path  $Q = q\Delta\Phi$ . The weighting potential as a function of position was found as the solution of the Laplace equation for the geometry of the detector with special boundary conditions. Evaluation of the ionization charge drift time can be done if the weighting potential inside the sensitive volume of the chamber is calculated as shown in the above graphs. Using explicit functions for weighting potential one can find the following expression for drift time  $T$  for ionization charge density shifting from the origin to the anode:

$$T = \frac{D}{W} \cdot \left\{ \left(1 - \frac{\bar{X}}{D} \cdot \cos(\Theta)\right) + \frac{d}{2 \cdot D} \cdot \left(1 - \frac{\sigma}{1 - \sigma}\right) \cdot \left(1 - \frac{\bar{X}}{D} \cos(\Theta)\right) \right\}, \text{ where the meanings of } d, D, \Theta \text{ are clear from}$$

the sketch of the TBIC,  $\sigma$  is the grid inefficiency factor or it is the value of the average weighting potential at grid location, and  $X$  is the center for ionization charge distribution along the FF track. Parameter  $T$  for corresponding anode can be measured using the signal current waveform as follows

$$T = S / S_0, \text{ where } S = \int_0^{T_{\max}} i(t) * t dt, S_0 = \int_0^{T_{\max}} i(t) dt$$

## 5. FF angle determination.



If the pulse height and drift time can be evaluated from anode signal waveform, then one can use them for fission fragment angle determination using the following formulas

$$T = \frac{D}{W} \cdot \left\{ \left(1 - \frac{\bar{X}}{D} \cdot \cos(\Theta)\right) + \frac{d}{2 \cdot D} \cdot \left(1 - \frac{\sigma}{1 - \sigma} \cdot \left(1 - \frac{\bar{X}}{D} \cos(\Theta)\right)\right) \right\}, \quad \cos(\Theta) = \frac{T_{90} - T}{T_{90} - T_0}, \text{ where}$$

$T_{90}, T_0$  - are drift times for cosine angles 90 and 0 degree respectively relative to the cathode plane normal, and  $T$  is the drift time for cosine angle  $\Theta$ . Well for cosine evaluation one first needs to determine the  $T_{90}, T_0$  - values from experimental data. To determine these values the following algorithm can be used. First the two dimensional plot of anode pulse height  $P$  versus drift time  $T$  is plotted and demonstrated in the upper graph. For fixed  $P$  the drift time, running from minimum value  $T_0$ , corresponding to 0 degree FF, up to maximum value  $T_{90}$ , corresponding to 90 degree FF. We implemented computer algorithm, where we first passing the plot  $F(P, T)$  through Gaussian shaped filter:

$$F'(P, T) = \int_0^{T_{\max}} (T - X) \cdot \exp\left(-\frac{(T - X)^2}{2S^2}\right) F(P, X) dX$$

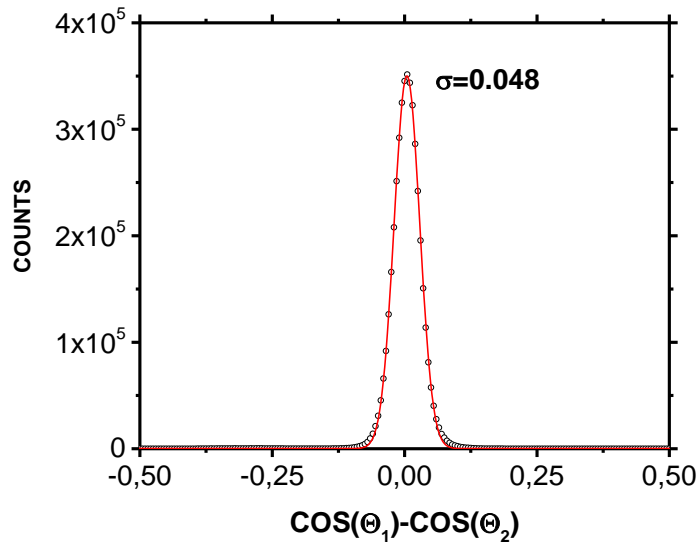
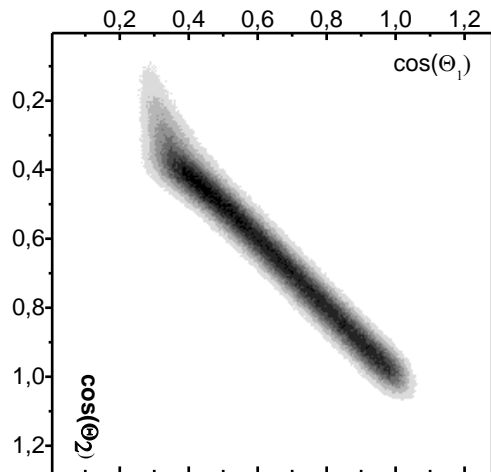
The middle graph demonstrates result of the filter application to the plot  $F(P, T)$ . It should be noted that the maximum  $T_{90}$ , and the minimum  $T_0$  values of drift time for the fixed value of the  $P$  can be found as the minimum and maximum values of vertical profile shown on the middle graph. When it was done and  $T_0$  was found for the whole range of pulse heights ( $T_{90}$  is constant independent on  $P$ ), then the cosine of  $\Theta$  can be evaluated for each FF and measured pulse height can be corrected for grid inefficiency using the following formula:

$$P_A^C = \frac{P_A}{1 - \sigma \left(1 - \frac{T}{T_{90}}\right) \cdot \left(1 + \frac{d}{2D}\right)}, \text{ where } P_A \text{ is the uncorrected}$$

and  $P_A^C$  is the corrected values of pulse height.

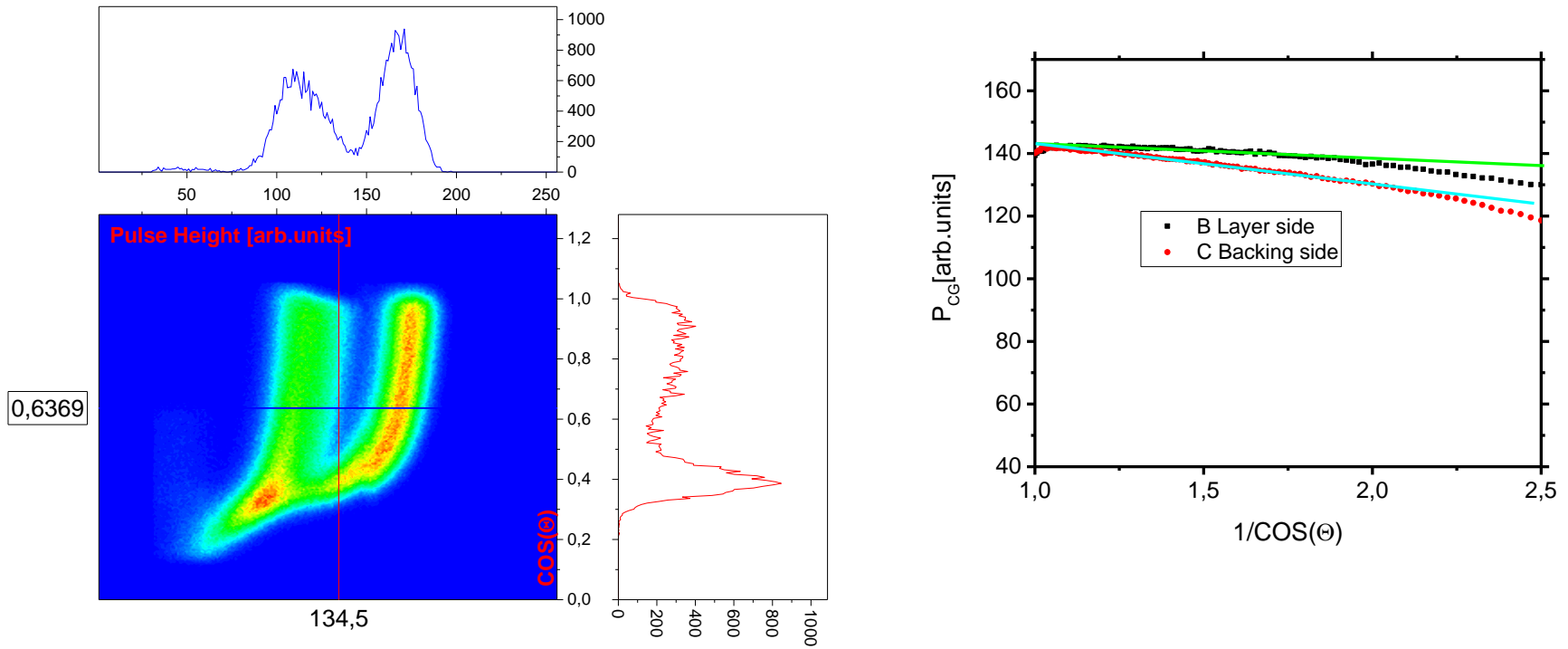


## Demonstration of $\cos(\Theta)$ evaluation



Cosine values determined according to the algorithm described in previous slide are plotted in two dimensional plot of cosines measured in both halves of TBIC. The left plot along with the right plot was used for adjusting of values found on both halves of the TBIC. This was done using iterative procedure minimizing the width and the slope of the track on the plot. Finally one should minimize the cosine uncertainty to the value  $\sim 0.05$

# Pulse height correction for energy losses in the target's layer and backing



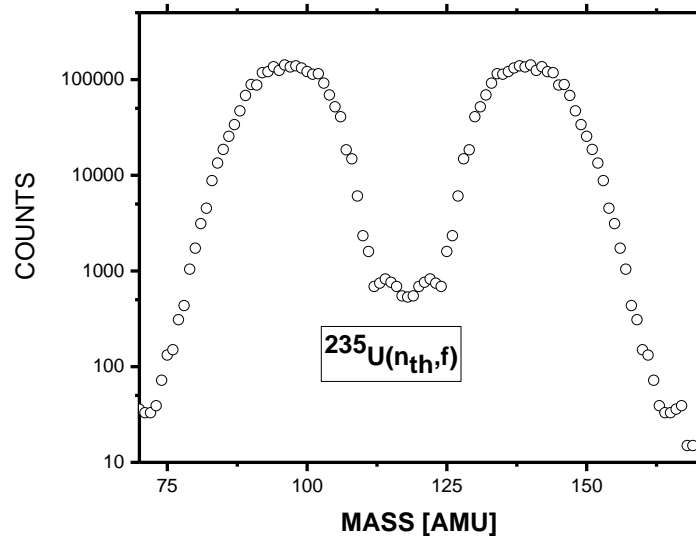
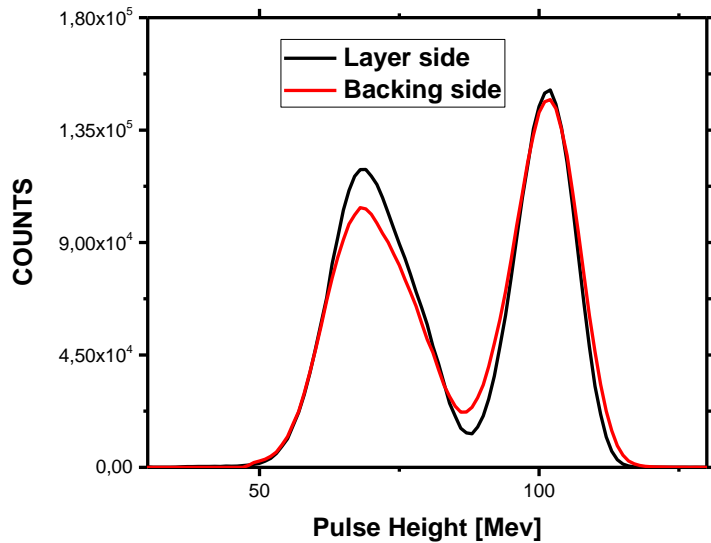
After the cosine value was determined the pulse height correction can be applied the pulse height versus cosine was plotted to find energy loss dependence on reverse cosine value was found and plotted on the right graph. In this work we use the algorithm as follows. Function  $H(P, \cos(\Theta))$  considered for fixed values  $\cos(\Theta) = \text{const}$  as one dimensional distribution as shown in the upper profile and two integrals were calculated

$$S = \int_{P_1}^{P_2} H(P, \cos(\Theta) = \text{const}) dP, \quad S1 = \int_{P_1}^{P_2} P \cdot H(P, \cos(\Theta) = \text{const}) dP$$

Then the energy correction values  $\Delta = \frac{S1}{S}$  found and plotted versus reverse cosine as demonstrated on the right plot for

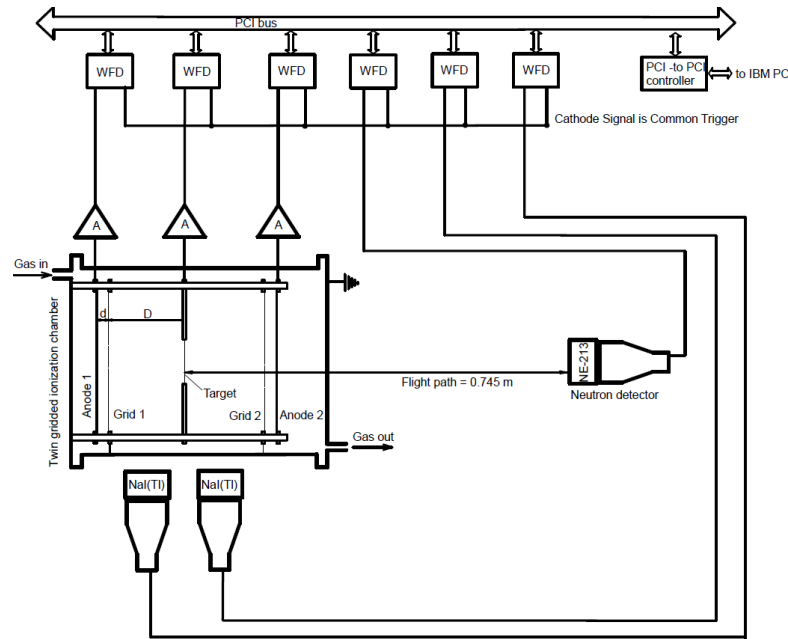
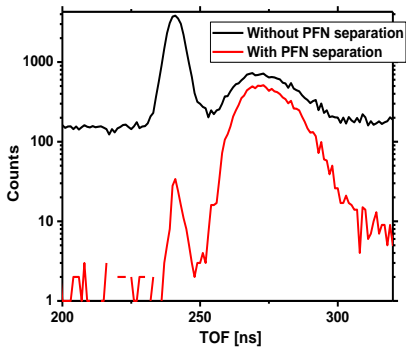
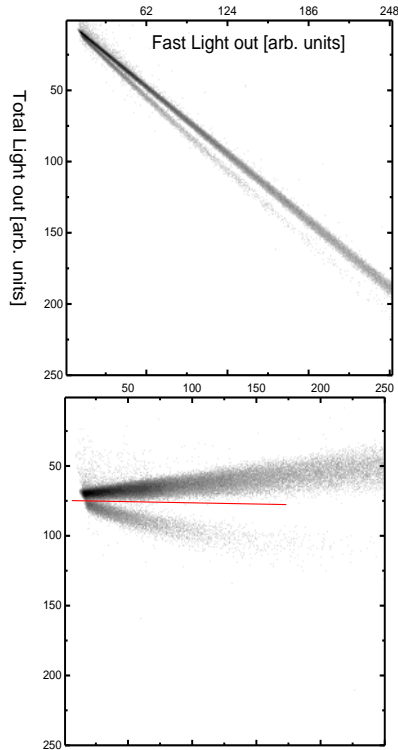
both sides of TBIC. The slopes are found as linear fit and assigned to pulse height correction value

## Calibration procedure



After pulse heights were corrected the FF kinetic energy values were calculated using two calibration parameters: one for the light fragment average kinetic energy and for TKE. The kinetic energy distributions for two sides are plotted on the left graph. The pre neutron emission masses of FF were calculated in the iterative procedure taking into account pulse height correction procedure described in literature Nuclear Instr. And Meth. A258 (1987) 209

# Neutron separation from gamma radiation

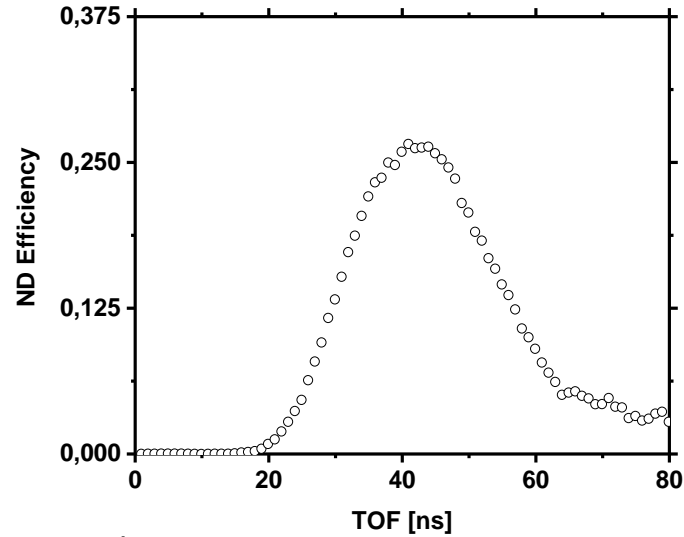
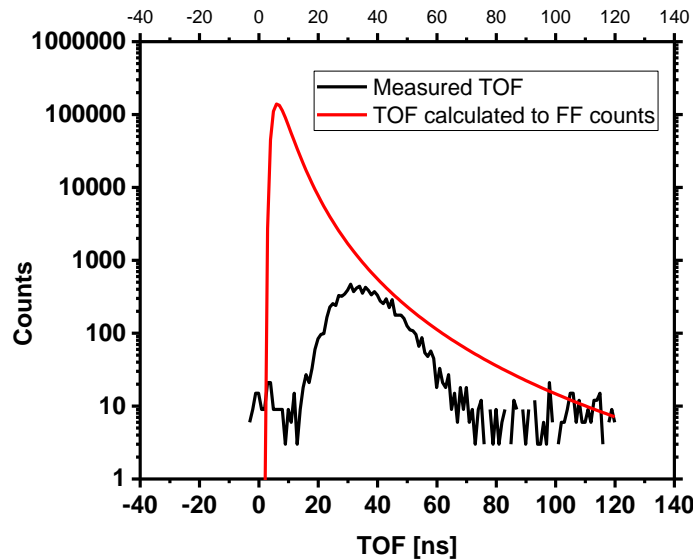


Then two window algorithm (fast and total light output component) was implemented and resulted function  $ND(FAST, TOTAL)$  was plotted on the upper and middle figs. demonstrates the function  $ND(FAST, TOTAL)$  in rotated according to equation

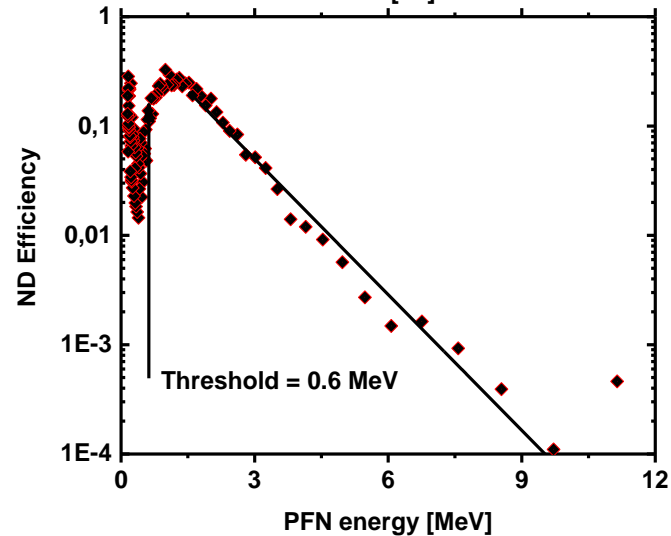
$$F' = F \cdot \cos(\Omega) + T \cdot \sin(\Omega), T' = S \cdot \{-F \cdot \sin(\Omega) + T \cdot \cos(\Omega)\}$$

where  $\Omega$  – is axes rotation angle and  $S > 1$  – is the scaling factor. Red line in the middle figure is PFN-PFG separation line. Lower figure demonstrates the TOF distribution before and after PFN separation.

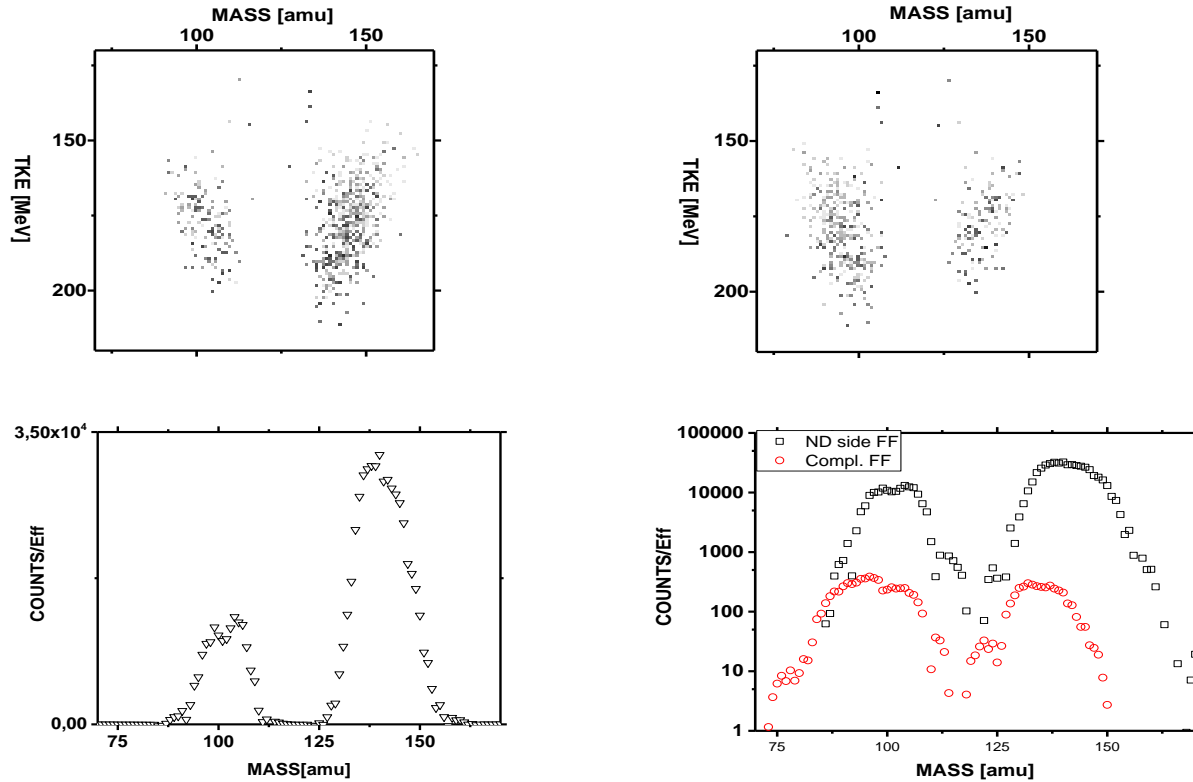
# ND Efficiency Evaluation



The total number of fission events used to measure the PFN coincidence was multiplied to  $\bar{\nu} = 2.01$  in order to obtain full number of PFN emitted during measurements. The energy spectrum of emitted PFN was supposed to be Maxwellian with temperature parameter  $kT = 1.313 \text{ MeV}$ . Measured TOF spectrum along with calculated Maxwellian TOF spectrum are plotted above. On the left we provided ND efficiency obtained as ratio of measured TOF to Maxwellian. The lower graph on the left is the energy dependence of ND efficiency

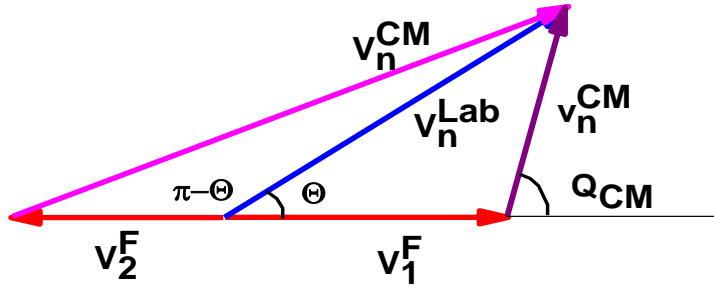


# PFN evaluation from measured data



The upper left plot demonstrates the measured  $v_f(A, TKE)$  matrix for FF moving in ND direction. The upper right plot demonstrates the similar  $v_b(A, TKE)$  matrix measured for the complementary FF. To measure these two distributions we followed the approach of C. Budtz-Jorgensen and H.-H. Knitter, assigning exponentially decaying with PFN energy waits as shown in the next slide

## PFN emission kinematics

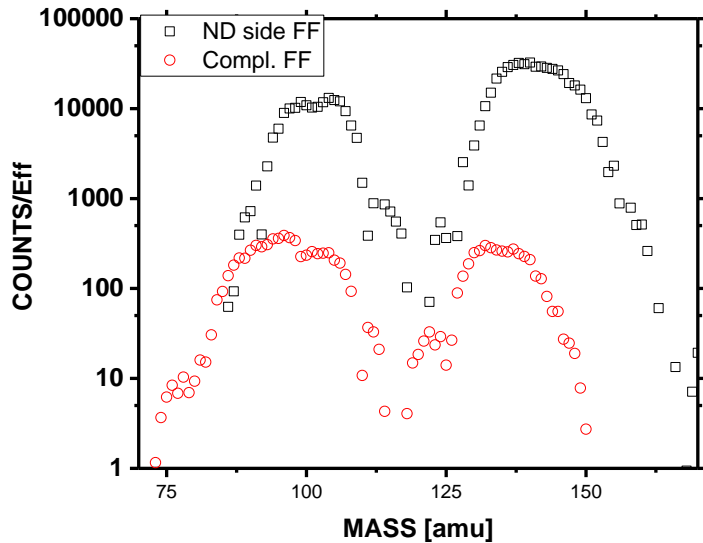


$$(V_n^{CM})^2 = (V_2^F)^2 + (V_n^{Lab})^2 + 2 \cdot V_2^F \cdot V_n^{Lab} \cdot \cos(\Theta)$$

$$(v_n^{CM})^2 = (V_1^F)^2 + (V_n^{Lab})^2 - 2 \cdot V_1^F \cdot V_n^{Lab} \cdot \cos(\Theta)$$

$$v_n^{CM} \cdot \cos(Q_{CM}) = V_n^{Lab} \cdot \cos(\Theta) - V_1^F$$

$$\Omega_{CM}(v_{CM}, \Theta_{CM}) dv_{CM} d\cos(\Theta_{CM}) = \frac{v_{CM}}{v_{lab}} \Omega_{lab}(v_{lab}, g(v_{CM}, \Theta_{CM}))$$



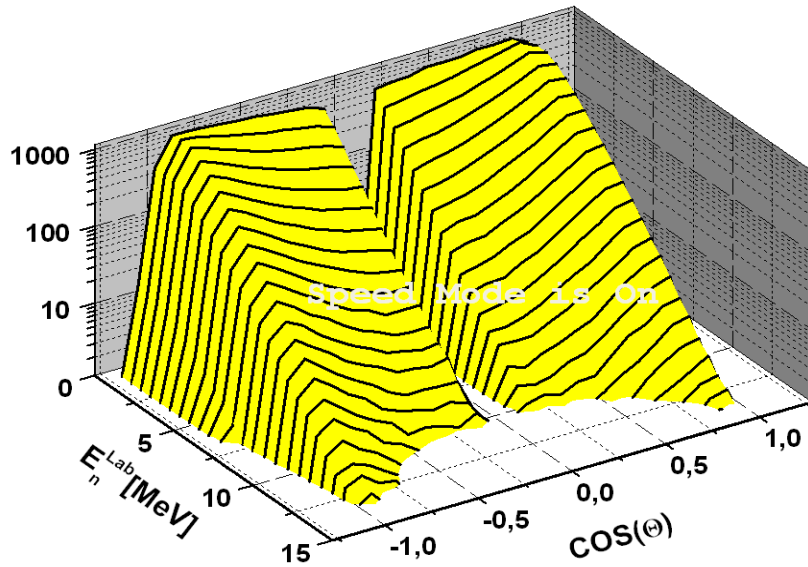
$$h_f = \left(\frac{1}{T}\right) \exp(-E_f^{CM} / T)$$

$$h_b = \left(\frac{1}{T}\right) \exp(-E_b^{CM} / T)$$

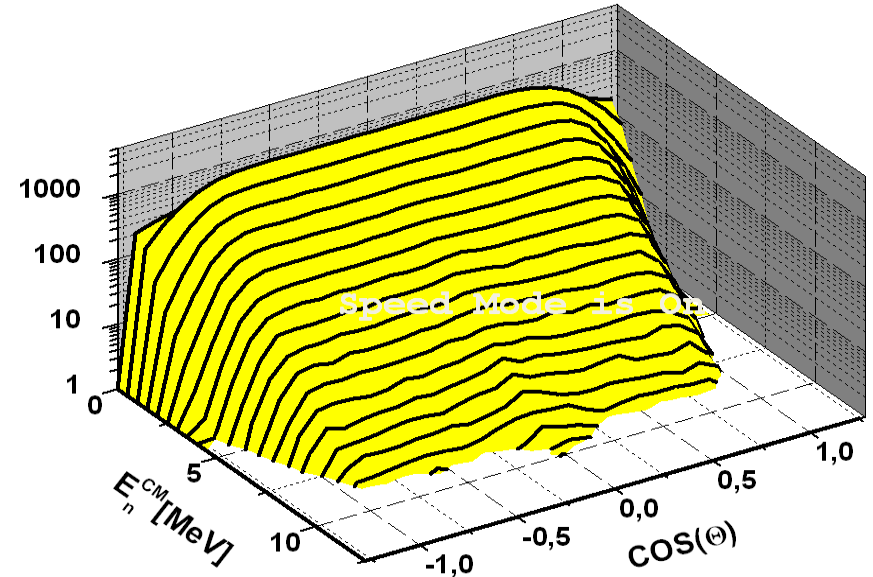
$$\alpha(h_f + h_b) = 1$$

where  $\alpha$  – normalization constant

# PFN angular distributions in Lab. And CM reference systems



Laboratory reference system



Centre-of-mass reference system

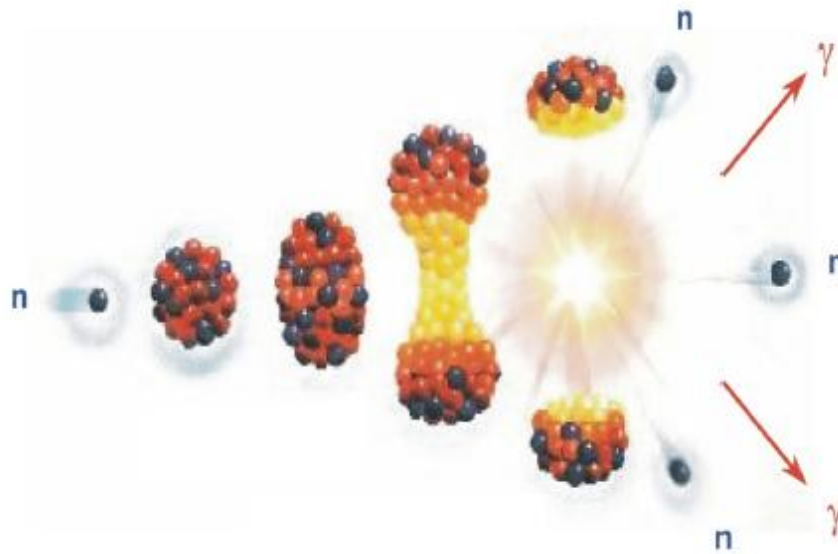


## Summary and conclusions

In this work we tried out to demonstrate the advantage of DPP approach over traditional analog one in experiment aimed the PFN emission investigation.

The experimental method pioneered by R. H. Bowman and later modified by C. Budtz-Jorgensen and H.-H. Knitter were further modified in our work thanks to flexibility and power provided by the digital signal processing. The progress in modern computer technology also was of great importance to improve the method.

The statistical accuracy of data (which is approximately 10% of acquired statistics) presented in this seminar was not enough to really demonstrate the full range of improvements we have achieved. But we just started data analysis and it is in progress.



**Thank you for your attention 😊**